

Data Repository for: Construction of the Lesser Himalayan-Subhimalayan thrust belt: the primary driver of thickening, high elevations, and exhumation in the Himalayan orogen since the middle Miocene

Figure DR1 (see accompanying oversized pdf): Compilation of 22 published cross sections across the Himalayan orogen, ordered from east to west (see Figure 1 in the main text for the locations of their lines of section). All cross sections are oriented with foreland-ward (i.e., toward the south in the eastern part of the orogen and toward the southwest in the western part of the orogen) toward the left-hand side. All structures shown in red are thrust faults with a top-up-toward-foreland (i.e., top-to-south in the eastern portion of the orogen and top-to-southwest in the western portion) motion sense. The top-down-toward-hinterland South Tibetan detachment system (STDS) and Zaskar shear zone (cross section 22 only) are shown in purple. Brittle normal faults with a top-down-toward-hinterland motion sense are shown in blue on cross sections 14, 16, 17, and 18. All cross sections are shown with the same unit color scheme, and all are shown at the same scale (1:1,253,133) with no vertical exaggeration.

Discussion DR1: Summary of tectonostratigraphic units in each cross section

1) Western Arunachal Pradesh cross section (DeCelles et al., 2016): Paleoproterozoic Lesser Himalayan (LH) rocks shown in dark blue include the ~1.86-1.81 Ga Shumar Formation, the ~1.81-1.77 Ga Bomdila orthogneiss, and the overlying Daling Formation (DeCelles et al., 2016). Neoproterozoic-Paleozoic LH rocks include quartzite, phyllite, and dolostone of the Neoproterozoic-Cambrian Rupa Group (DeCelles et al., 2016), which are likely correlative to the Baxa Group of Bhutan (Long et al., 2011), and quartzite of the Upper Paleozoic Miri Formation, Permian Diuri Formation, and Permian Gondwana unit in foreland thrust sheets (DeCelles et al., 2016). In addition, garnet-bearing schist, quartzite, and marble of the Neoproterozoic-Cambrian Jaishidanda Formation is exposed in two thrust sheets under the Main Central thrust (MCT). Unlike in Bhutan, where the Jaishidanda Formation is mapped as stratigraphically overlying the

Daling Formation, the base of the Jaishidanda Formation is mapped as a thrust fault in western Arunachal Pradesh (DeCelles et al., 2016), bringing the tectonostratigraphic affinity of this unit into question. DeCelles et al. (2016) interpreted the Jaishidanda Formation to possibly be a lower-grade unit of GH affinity; however, they still mapped the Main Central Thrust at the top of the Jaishidanda Formation. The Jaishidanda Formation does not have an equivalent LH unit exposed further to the south in the LH thrust belt, similar to the interpretation of the Paro Formation in western Bhutan by McQuarrie et al. (2014). In accordance with our treatment of the rest of the cross sections across the orogen, we group any rocks below the MCT as being part of the LH thrust belt. Thus, similar to the interpretation made for the Paro Formation in western Bhutan by McQuarrie et al. (2014), we interpret that the Jaishidanda Formation in Arunachal Pradesh represents rocks below the MCT that restore to a distal position to the north of restored LH rocks, but to the south of the restored position for Greater Himalayan (GH) rocks (as shown in DeCelles et al., 2016). Keeping in accordance with our treatment of the rest of the cross sections across the orogen, we use the mapped position of the MCT on the cross section of DeCelles et al. (2016) to determine the dividing line between the GH section and the LH thrust belt. Thus, on our simplified cross section compilation, we interpret the Jaishidanda Formation in western Arunachal Pradesh as technically being of LH affinity, as it is mapped as underlying the MCT. Mesozoic-Paleogene LH rocks shown in orange include the Cretaceous-Paleocene ('KT') unit, consisting of sandstone and carbonaceous shale that is tentatively correlated with the Amile Formation in Nepal, which is overlain by sandstone that is tentatively interpreted as correlative to the lower Miocene Dumri Formation in Nepal (DeCelles et al., 2016). Subhimalayan (SH) rocks shown in yellow include the middle Miocene-Pliocene Siwalik Group (DeCelles et al., 2016). GH rocks shown in pink include Neoproterozoic-Ordovician, high-grade, kyanite- or sillimanite-bearing schist, paragneiss, leucogranite, and migmatite (DeCelles et al., 2016). Tethyan Himalayan rocks include undifferentiated metasedimentary rocks on the northern edge of the cross section, above the STDS (DeCelles et al., 2016).

2) Sakteng cross section, easternmost Bhutan (McQuarrie et al., 2019), 3) Trashigang and 4) Kuru Chu cross sections, eastern Bhutan (Long et al., 2011a), and 5) Bumthang Chu and 6) Mangde Chu cross sections, central Bhutan (Long et al., 2011a): Paleoproterozoic LH rocks shown in dark blue include quartzite and phyllite of the ~1.8-1.9 Ga Daling-Shumar Group

and interlayered orthogneiss (Long et al., 2011a). Orthogneiss interlayers become thicker and more common in easternmost Bhutan (McQuarrie et al., 2019). Neoproterozoic-Paleozoic LH rocks shown in light blue include quartzite and phyllite of the Neoproterozoic-Cambrian Manas Formation of the Baxa Group, which is exposed across the width of Bhutan, as well as diamictite of the Permian Diuri Formation and sandstone and shale of the Permian Gondwana succession, which are only exposed in eastern Bhutan (Long et al., 2011a). In addition, the Neoproterozoic-Ordovician Jaishidanda Formation stratigraphically overlies the Daling-Shumar Group and underlies the MCT across the width of Bhutan (Long et al., 2011a), and is also included in our light blue LH unit. SH rocks shown in yellow include the Miocene-Pliocene Siwalik Group, which are exposed in a single thrust sheet above the MCT across central and eastern Bhutan (Long et al., 2011a). GH rocks shown in pink consist of upper amphibolite-facies, locally migmatitic metasedimentary rocks with Neoproterozoic-Ordovician protoliths that are intruded by Cambrian-Ordovician granitic orthogneiss below the Kakthang thrust, and amphibolite- to granulite-facies, migmatitic metasedimentary rocks, orthogneiss, and Miocene leucogranite above the Kakthang thrust (Long et al., 2011a; 2011b). Tethyan Himalayan rocks (shown in green) in central and eastern Bhutan include garnet-bearing schist and quartzite of the basal, Ordovician (or younger) Chekha Formation, which is overlain in one locality in central Bhutan by greenschist-facies metasedimentary rocks as young as Carboniferous (Long et al., 2011a; 2011b). Several isolated exposures of the Chekha Formation have been mapped in central and eastern Bhutan; however, whether or not they are all underlain by the STDS is debated (e.g., see summary in Long et al., 2017).

7) Wang Chu cross section, Western Bhutan (McQuarrie et al., 2014): Paleoproterozoic LH rocks shown in dark blue include quartzite and phyllite of the ~1.8-1.9 Ga Daling-Shumar Group (Long et al., 2011b). Neoproterozoic-Paleozoic LH rocks (shown in light blue) include the Baxa Group (in foreland thrust sheets below the Shumar thrust), which consists of the Pangsari, Manas, and Phuentsholing Formations (McQuarrie et al., 2014). The Manas and Phuentsholing Formations in western Bhutan are no older than Neoproterozoic, although the underlying Pangsari Formation could be as old as Mesoproterozoic (Long et al., 2011b). Below the foreland-ward exposure of the MCT, the Neoproterozoic-Ordovician Jaishidanda Formation stratigraphically overlies the Daling-Shumar Group and is also included in our light blue LH unit

(McQuarrie et al., 2014). Further to the north on the cross section, the Neoproterozoic-Ordovician Paro Formation is exposed in a window beneath a shear zone that is mapped as a northern continuation of the MCT, and is interpreted by McQuarrie et al. (2014) to be of LH affinity; therefore, after these interpretations, we include the Paro Formation as part of our light blue LH unit. However, the ~5 km-thick Paro Formation does not have an equivalent stratigraphic unit in the LH thrust belt further to the south (it is possibly correlative in time with the Jaishidanda Formation, although this cannot be demonstrated with confidence; e.g., Long et al., 2011b). Therefore, McQuarrie et al. (2014) interpreted the Paro Formation as a rock unit of LH affinity that restores to a distal position, northward of the restored positions of LH thrust sheets that are exposed below the MCT in the foreland. SH rocks that are shown in yellow include the Miocene-Pliocene Siwalik Group, which are poorly exposed in western Bhutan and are interpreted to overlie the MFT, as demarcated by uplifted and incised river terraces (McQuarrie et al., 2014). GH rocks shown in pink include upper amphibolite-facies, locally migmatitic metasedimentary rocks with Neoproterozoic-Ordovician protoliths, which are intruded by Cambrian-Ordovician granitic orthogneiss (Long et al., 2011b). Tethyan Himalayan rocks shown in green include Paleozoic to Mesozoic marble, quartzite, slate, limestone, and sandstone above the STDS in northwestern Bhutan (Long et al., 2011b).

8) Eastern Sikkim cross section (Parui and Bhattacharyya, 2018), and 9) Western Sikkim cross section (Bhattacharyya et al., 2015): Paleoproterozoic LH rocks shown in dark blue include the ~1.8-1.9 Ga Paro Formation (or Paro Gneiss or Paro Paragneiss) and interlayered ~1.83 Ga Lingtse Gneiss (or Lingtse Orthogneiss), which are carried in a sheet bound above by the MCT and bound below by the Pelling thrust, and the Daling Group (which is interpreted to correlate with the ~1.8-1.9 Ga Daling-Shumar Group of Bhutan), consisting of a lower quartzite unit and an upper phyllite unit (Bhattacharyya et al. 2015; Parui and Bhattacharyya, 2018). Based on its structural position in the LH thrust belt, we interpret that the Pelling thrust is likely correlative to the Ramgarh thrust mapped further to the west in Nepal. The Paro Formation/Lingtse Gneiss are interpreted to restore stratigraphically below the Daling Group (Bhattacharyya et al., 2015; Parui and Bhattacharyya, 2018). Based on its Paleoproterozoic age, the Paro Formation in Sikkim is not correlative with the Neoproterozoic-Ordovician (or younger) Paro Formation mapped in western Bhutan (McQuarrie et al., 2014). Neoproterozoic-Paleozoic

LH rocks in Sikkim (shown in light blue) include the Neoproterozoic-Early Cambrian Buxa Group (or Buxa Formation) (Bhattacharyya et al., 2015), which is interpreted to correlate with the Neoproterozoic-Cambrian Buxa Group of Bhutan (Long et al., 2011a), and the Permian Gondwana Formation (or Gondwana Group) (Parui and Bhattacharyya, 2018). SH rocks shown in yellow include the Miocene-Pliocene Siwalik Group. GH rocks shown in pink include the granulite-facies, sillimanite- and kyanite-bearing, migmatitic, Neoproterozoic Kanchenjunga/Darjeeling Gneiss, which overlies the MCT (Bhattacharyya et al., 2015). Tethyan Himalayan rocks shown in green include undifferentiated Paleozoic-Mesozoic low-grade metasedimentary rocks above the STDS on the northern edge of the cross sections.

10) Tamor Khloa cross section (Schelling, 1992), and 11) Ramechap cross section

(Schelling, 1992), eastern Nepal: Very few constraints on the depositional ages of LH rocks were available at the time of publication of Schelling and Arita (1991) and Schelling (1992), and their use of local formation names makes correlation with LH units to the west and east difficult. The LH section in eastern Nepal (from stratigraphically lowest to highest) consists of the Taplejung Group, Tumlingtar Group, and Ramechap Group (which are interpreted by Schelling, 1992, as lateral equivalents of each other), the Suri Dhoban augen gneiss, the Dolakha phyllite, and the overlying Melung-Salleri, Khandbari, and Sisne Khola augen gneiss units, which are interpreted to be equivalent to the Paleoproterozoic (~1.83 Ga) Ulleri augen gneiss mapped further to the west in Nepal (Schelling, 1992). Therefore, we interpret that all LH rocks including and below this augen gneiss unit are most likely Paleoproterozoic in age, and we group them together into our dark blue Paleoproterozoic LH unit. Above the augen gneiss, a <1 km-thick phyllite unit is exposed and is named the Sun Kosi phyllite toward the foreland and the Khare phyllite toward the hinterland; these two units are interpreted as lateral equivalents of each other (Schelling, 1992). The Khare phyllite has yielded paleobasidiospores that have been interpreted to be as young as Cambrian (Schelling, 1992). Therefore, we show the Sun Khosi and Khare phyllite units as a thin layer that is part of our light blue Neoproterozoic-Paleozoic LH unit. SH rocks shown in yellow include the Miocene to Pleistocene Siwalik Group (Schelling and Arita, 1991; Schelling, 1992). GH rocks shown in pink include the ‘Higher Himalayan Crystallines’, consisting of migmatitic, Cambrian-Ordovician granitic orthogneiss, sillimanite- and locally

kyanite-bearing paragneiss and schist, metaquartzite, marble, and amphibolite, with Miocene leucogranites at the highest structural levels (Schelling and Arita, 1991; Schelling, 1992).

12) Budhi Gandaki, Central Nepal (Khanal and Robinson, 2013): Paleoproterozoic LH rocks shown in dark blue include the <1.9 Ga Kuncha Formation, the Robang Formation (which contains the Dunga Quartzite), the <1.8 Ga Fagfog Formation, and the Dandagaon Formation (Khanal and Robinson, 2013). Mesoproterozoic LH rocks shown in purple include the <1.68 Ga Norpoul Formation and the >1.25 Ga Benighat, Dhading, and Malekhu Formations (Martin et al., 2011; Khanal and Robinson, 2013). Mesozoic-Paleogene LH units shown in orange include the ‘Gondwana and Tertiary’ unit (Khanal and Robinson, 2013). SH rocks shown in yellow include the middle Miocene to Pliocene Siwalik Group (Khanal and Robinson, 2013). GH rocks shown in pink include two separate exposures of Neoproterozoic-Ordovician metasedimentary rocks; in the Kathmandu Klippe on the south these rocks are chlorite- to garnet-grade, and on the northern end of the cross section these rocks are amphibolite to granulite grade (Units I, II, and III) (Khanal and Robinson, 2013). Tethyan Himalayan rocks shown in green include the Cambrian(?) Sanctuary Formation above the STDS (Khanal and Robinson, 2013).

13) Marsyangdi, Central Nepal (Khanal, 2014): Paleoproterozoic LH rocks shown in dark blue include the <1.9 Ga Kuncha Formation, the <1.85 Ga Robang Formation, the <1.77 Ga Fagfog Formation, and the Dandagaon Formation (Martin et al., 2011; Khanal, 2014). Mesoproterozoic rocks shown in purple include the <1.68 Ga Norpoul Formation, the Dhading Formation, the Benighat Formation, and the >1.3 Ga Malekhu Formation (Martin et al., 2011; Khanal, 2014). Mesozoic-Paleogene rocks shown in orange include the ‘Gondwana and Tertiary’ unit (Khanal, 2014). SH rocks shown in yellow include the Miocene-Pleistocene Siwalik Group (Khanal, 2014). GH rocks shown in pink consist of amphibolite- to granulite-facies metasedimentary and meta-igneous rocks with Neoproterozoic-Ordovician protoliths (Khanal, 2014).

14) Kaligandaki, Central Nepal (Robinson and Martin, 2014) (note: their cross section 1 was utilized in our study): Paleoproterozoic LH rocks shown in dark blue include the ~1.9-1.78 Ga Kuncha Formation (Martin et al., 2011), the <1.77 Ga Fagfog Formation (Martin et al.,

2011), and the Galyang Formation (Robinson and Martin, 2014). Mesoproterozoic LH rocks shown in purple include the <1.68 Ga Syangja Formation (equivalent to the Norpoul Formation), and the >1,300 Ma Dhading, Malekhu, and Benighat Formations (Martin et al., 2011; Robinson and Martin, 2014). Mesozoic-Paleogene LH rocks include the Mesozoic to Paleocene Gondwana Sequence, the Paleocene-Eocene Bhainskati Formation, and the early Miocene Dumri Formation (Robinson and Martin, 2014). Neogene SH rocks shown in yellow include the middle Miocene to Pliocene Siwalik Group (Robinson and Martin, 2014). GH rocks shown in pink include metasedimentary rocks and Cambrian-Ordovician orthogneiss of Units I, II, and III (Robinson and Martin, 2014).

15) Simikot, 16) Chainpur, and 17) Api cross sections, Western Nepal (Robinson et al., 2006): Paleoproterozoic LH rocks shown in dark blue include the ~1.85 Ga Kushma Formation, Ranimata Formation, ~1.83 Ga Ulleri augen gneiss, the <1.74 Ga Sangram Formation, and Galyang Formation (Robinson et al., 2006). Mesoproterozoic LH rocks shown in purple include the <1.68 Ga Syangja/Blaini Formation (equivalent to the Norpoul Formation of central Nepal) and the >1,300 Ma Lakharpata Group (equivalent to the Benighat, Dhading, and Malekhu Formations of central Nepal; Robinson and Martin, 2014). Mesozoic-Paleogene LH rocks shown in orange include the Eocene Bhainskati Formation and the lower Miocene Dumri Formation (Robinson et al., 2006). Neogene SH rocks shown in yellow include the Miocene-Pleistocene Siwalik Group (Robinson et al., 2006). GH rocks shown in pink include metasedimentary and meta-igneous rocks (including Cambrian-Ordovician orthogneiss) in the Dadeldhura klippe toward the foreland, and a north-dipping section of upper amphibolite-facies, Neoproterozoic-Ordovician metasedimentary and meta-igneous rocks in the hinterland consisting of Formations I, II, and III (Robinson et al., 2006). Tethyan Himalayan rocks shown in green (shown on the Chainpur and Api cross sections only) consist of low-grade metasedimentary rocks above the STDS that are likely Cambrian-Ordovician in age (Robinson et al., 2006). Paleozoic Tethyan Himalayan rocks are also mapped above GH rocks in the Dadeldhura klippe on the Api cross section, although the nature of this contact (stratigraphic versus structural, i.e., whether or not it represents an exposure of the STDS) is debated (e.g., Robinson et al., 2006).

18) Eastern Kumaun cross section (Mandal et al., 2019): Paleoproterozoic LH rocks shown in dark blue include the Ramgarh-Berinag-Munsiari Formations and associated ~1.85 Ga granitic orthogneiss bodies (Mandal et al., 2019). Mesoproterozoic LH rocks shown in purple include the Rautgura Formation/Chakrata Formation (~1600 Ma) (Mandal et al., 2019). Neoproterozoic-Paleozoic LH rocks shown in light blue include the <950 Ma Deoban-Mandali Formation, the <800 Ma Chandpur Formation, the Nagthat Formation, the Cryogenian Blaini Formation, the Ediacaran Krol Formation, and the Lower Cambrian Tal Formation (Mandal et al., 2019). Neogene SH rocks shown in yellow include the Miocene Lugad Gad Formation and the Miocene-Pleistocene Siwalik Group (Mandal et al., 2019). GH rocks shown in pink include Neoproterozoic-Ordovician amphibolite- to granulite-facies metasedimentary and meta-igneous rocks of the Vaikrita Group carried above the MCT within the Almora Klippe and in the hinterland part of the cross section (Mandal et al., 2019). Tethyan Himalayan rocks shown in green consist of the Martoli Formation and Budhi schist of the Haimantas carried above the STDS (Mandal et al., 2019).

19) Almora, and 20) Deoprayag cross sections, Kumaun and Garwhal (Srivastava and Mitra, 1994): Paleoproterozoic LH rocks shown in dark blue include the Damta Group (Paleoproterozoic; Webb, 2013), a sheet of the Ramgarh Group carried by the Ramgarh thrust (Almora cross section only), and a sheet of overlying amphibolite-facies metasedimentary rocks and ~1.87 Ga granitic orthogneiss of the Almora Group that is carried by the Munsiari thrust and underlies the MCT (Srivastava and Mitra, 1994). The Ramgarh Group and Almora Group are likely correlative to the Paleoproterozoic Munsiari Formation mapped in eastern Kumaun by Mandal et al. (2019). Neoproterozoic-Paleozoic LH rocks shown in light blue include the Deoban Group (Neoproterozoic or younger; Mandal et al., 2019) and overlying Berinag Formation in hinterland thrust sheets, and the Chandpur Formation (Neoproterozoic; Mandal et al., 2019), Nagthat Formation (Neoproterozoic; Mandal et al., 2019), Blaini Formation (Neoproterozoic; Webb, 2013), Krol Group (latest Neoproterozoic; Webb, 2013), and Tal Formation (Lower Cambrian; Webb, 2013) in foreland thrust sheets. Mesozoic-Paleogene LH rocks shown in orange include the Paleocene-Eocene Subathu Formation (Srivastava and Mitra, 1994). Neogene rocks shown in yellow include the lower, middle, and upper units of the Miocene-Pleistocene Siwalik Group (Srivastava and Mitra, 1994). GH rocks shown in pink

include amphibolite- to granulite-facies metasedimentary and meta-igneous rocks of the Vaikrita Group that overlie the MCT (commonly referred to as the Higher Himalayan Crystallines in adjacent areas of northwestern India) (Srivastava and Mitra, 1994). Tethyan Himalayan rocks (shown only on the Almora cross section) include Neoproterozoic, Paleozoic, and Mesozoic sedimentary rocks above the STDS (called the Malari fault in Srivastava and Mitra, 1994).

21) Himachal Pradesh cross section (Webb, 2013): Paleoproterozoic LH rocks shown in dark blue include units Xw/Xj (the Wangtu and Jeori Formations of the Munsiri Group), XBe (the Berinag Group), and XD (the Damtha Group) (Webb, 2013). Neoproterozoic-Paleozoic LH rocks shown in light blue include unit Y-Z (Deoban Group), and three units of the ‘Outer Lesser Himalaya’, ZB (Basantpur Formation), ZS (Shimla Group), and Z-Ck (Krol Group) (Webb, 2013). Mesozoic-Paleogene LH rocks shown in orange include unit K/E (Paleocene-Eocene Subathu Formation) (Webb, 2013). Neogene SH rocks shown in yellow include units Mld (Miocene Lower Dharamsala Formation), Mud (Miocene Upper Dharamsala Formation), Mls (Miocene Lower Siwalik Formation), MMs (Miocene Middle Siwalik Formation), and M-Q (Miocene to Pleistocene Upper Siwalik Formation) (Webb, 2013). GH rocks shown in pink include unit Z-CGHC (Greater Himalayan Crystalline Complex; Neoproterozoic-Cambrian protoliths) (Webb, 2013). Tethyan Himalayan rocks shown in green include units C-O (Cambrian-Ordovician granites just above the STDS), Z-CH (Cambrian Haimanta Group), Cp (Cambrian Parahio Formation), O-C (Ordovician to Carboniferous Thaple-Muth-Lipak succession), and P-J (Permian to Jurassic Tandi Group) (Webb, 2013).

22) Eastern Kashmir cross section (Gavillot et al., 2018): Paleoproterozoic LH rocks shown in dark blue include undifferentiated ‘Lesser Himalaya units’ below the MCT and in the Kishtwar Window that lack depositional age control and are described as Precambrian to possibly Paleozoic in age (Gavillot et al., 2018). Neoproterozoic-Paleozoic LH rocks shown in light blue include the Sirban Limestone, which has a likely Neoproterozoic depositional age (Bhat et al., 2009). Mesozoic-Paleogene LH rocks shown in orange include the Paleocene-Eocene Subathu Formation and the Oligocene Lower Murree Formation (Gavillot et al., 2018). Neogene SH rocks shown in yellow include the Lower Miocene Upper Murree Formation and four Siwalik Group units that range in age from Lower Miocene to Pleistocene (Gavillot et al., 2018). GH

rocks shown in pink include a thin sheet of low-medium grade Haimantas just above the MCT (the ‘Kashmir-Chamba Nappe’) and a thick sheet of high-grade Haimantas (the High Himalayan Crystallines) (Gavillot et al., 2018). Tethyan Himalayan rocks shown in green include undifferentiated Paleozoic-Mesozoic strata above the Zaskar Shear Zone (Gavillot et al., 2018).

Table DR1 (see accompanying Excel table): Summary of published shortening estimates for the LH-SH thrust belt, LH-SH accreted area measurements, minimum structural overlap estimates for the MCT, and the structural thickness of GH rocks from the 22 compiled cross sections. Footnotes give details on values that we measured from cross section figures in the source publications, or on values reported here that deviate from those presented in the source publications. LH-SH accreted area estimates were measured by tracing polygons of the total (i.e., above and below the modern surface; this still represents a minimum estimate, as the leading portions of LH and SH thrust sheets are eroded in the frontal imbricate zone on virtually all cross sections) and preserved (i.e., below the modern surface) areas of LH-SH rocks in Adobe Illustrator, importing these polygons into the open-source software program Image J (Schneider et al., 2012), assigning a scale, and using the ‘area’ function. LH – Lesser Himalayan; GH – Greater Himalayan; SH – Subhimalayan.

Table DR2 (see accompanying Excel table): Summary of calculations of the surface slope angle (α), basal décollement angle (β), and taper angle ($\alpha + \beta$) for each cross section. Elevation and depth measurements from each cross section that were used to support these calculations are shown in Table DR4.

Figure DR2: Graphs of elevation versus distance north of the MFT trace and corresponding best-fit trendlines used to calculate the surface slope angle (α) for each cross section.

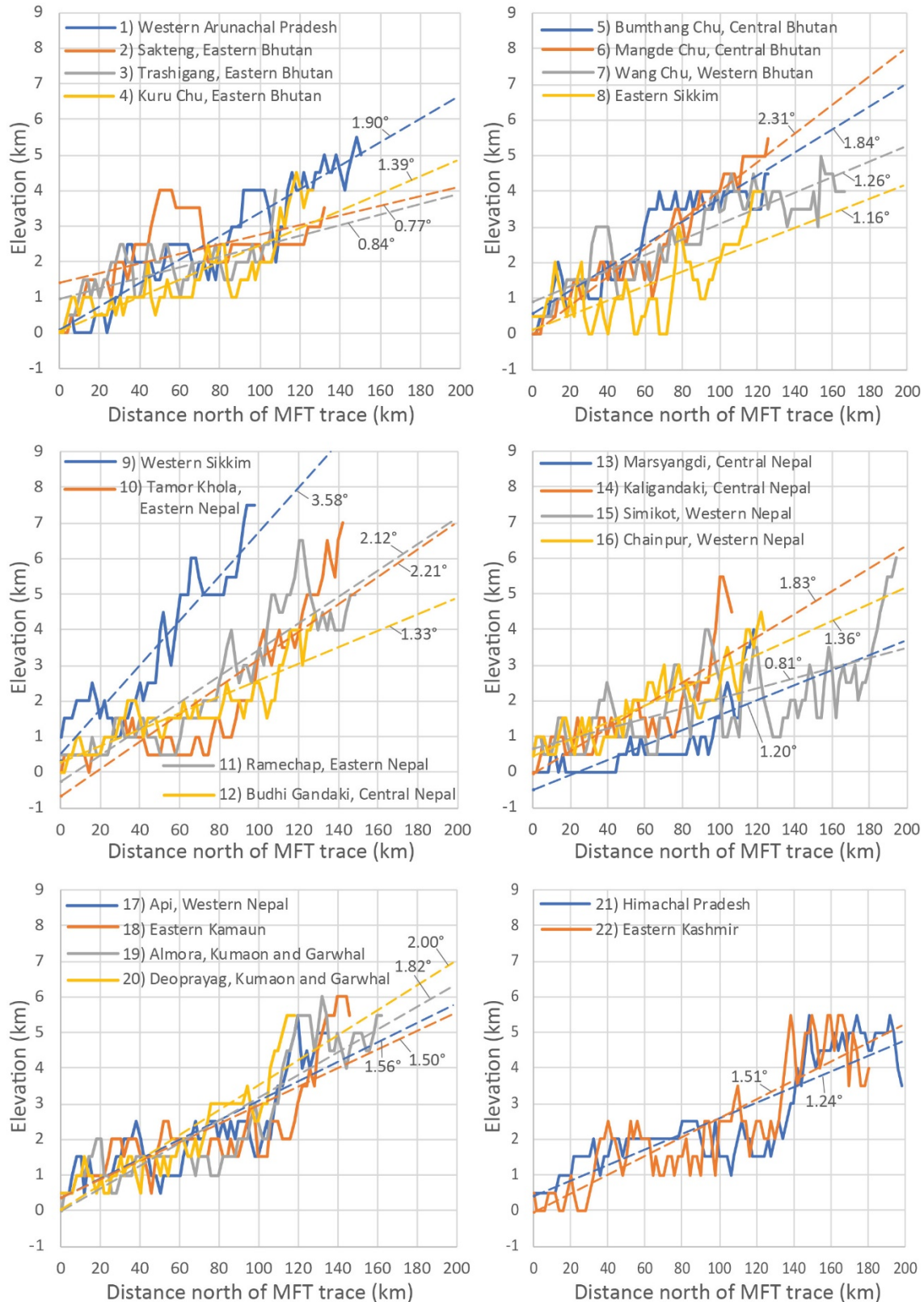


Figure DR3: Graphs of depth to the basal décollement versus distance north of the MFT trace and corresponding best-fit trendlines used to calculate the surface slope angle (β) for each cross section.

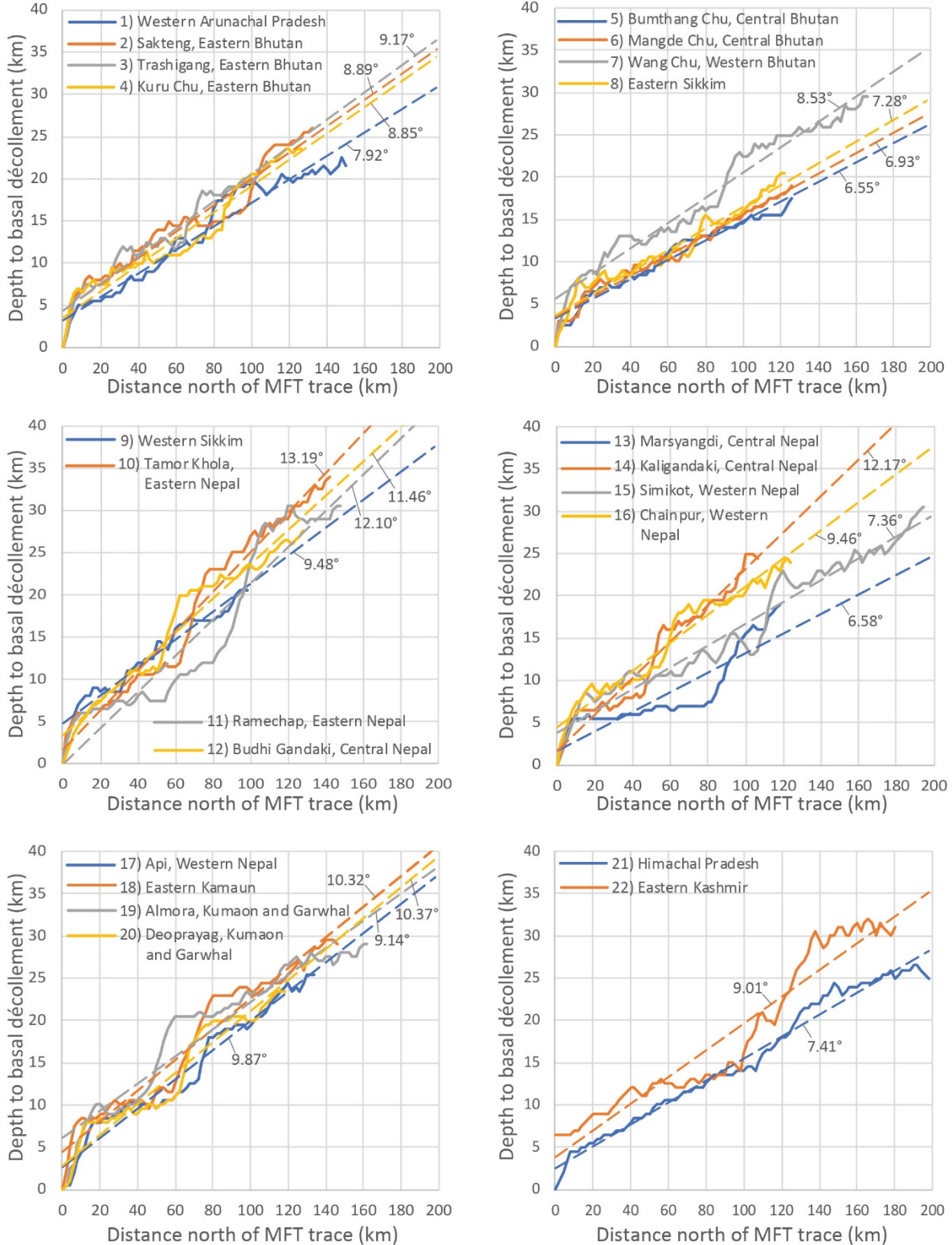


Table DR3 (see accompanying Excel table): Summary of measurements of the southern extent (the southern tip of the forelimb, where the MCT reaches its lowest structural elevation), peak location, northern extent (the location where the basal elevation of the forelimb intersects the MCT; see Figure 2 inset in the main text), north-south width, peak height (elevation of the peak compared to the basal elevation of the MCT in the forelimb), and area (measured between the MCT and the basal elevation of the forelimb; measured using Image J, utilizing the same methods as described above for LH-SH accreted area estimates) for the LH structural culmination on each of the 22 cross sections.

Table DR4 (see accompanying Excel table): Measurements of surface elevation, the depth to the basal décollement, total LH-SH structural elevation (measured by comparing the elevation of the structurally highest LH-SH stratigraphic contact above or below the modern surface to its elevation beneath the basal décollement), and preserved LH-SH structural elevation (measured by comparing the elevation of the LH-SH stratigraphic level exposed at the modern surface to its elevation below the basal décollement), for each of the 22 compiled cross sections. All measurements were collected at an interval of 2 km, with the MFT trace as the ‘0’ reference point for the deformation front. The reference stratigraphic contact used to measure total LH-SH structural elevation is listed for each datapoint, as well as the locations of the traces of major structures (see individual source publications for rock unit and structure abbreviations).

Figure DR4: Graphs of the total structural elevation (measured by comparing the elevation of the structurally highest LH-SH stratigraphic contact above or below the modern surface to its elevation at or beneath the basal décollement; see Fig. 2 inset) accomplished by construction of the LH-SH thrust belt versus distance north of the MFT trace for each of the 22 cross sections. The data used to make these graphs are shown in Table DR4.

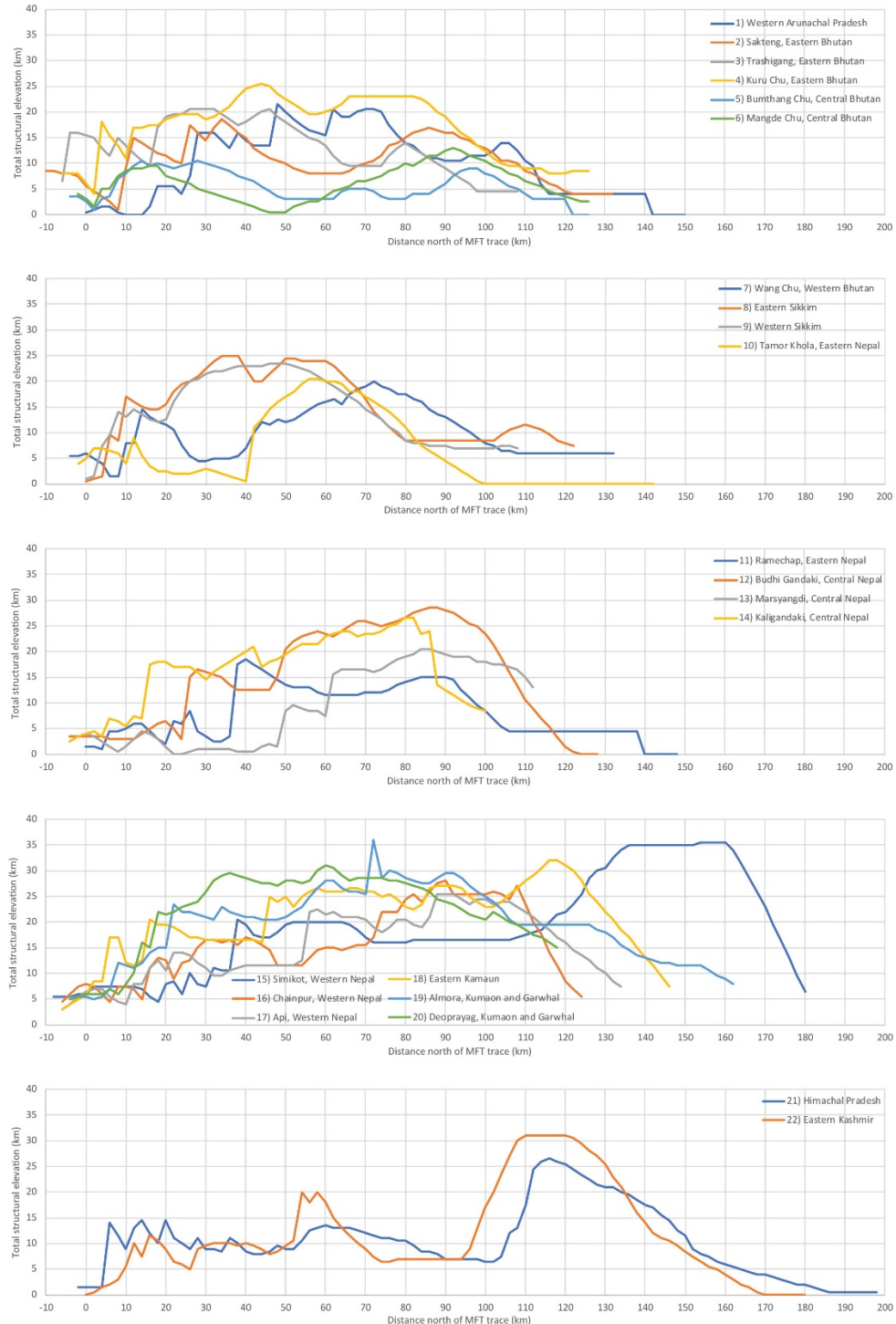
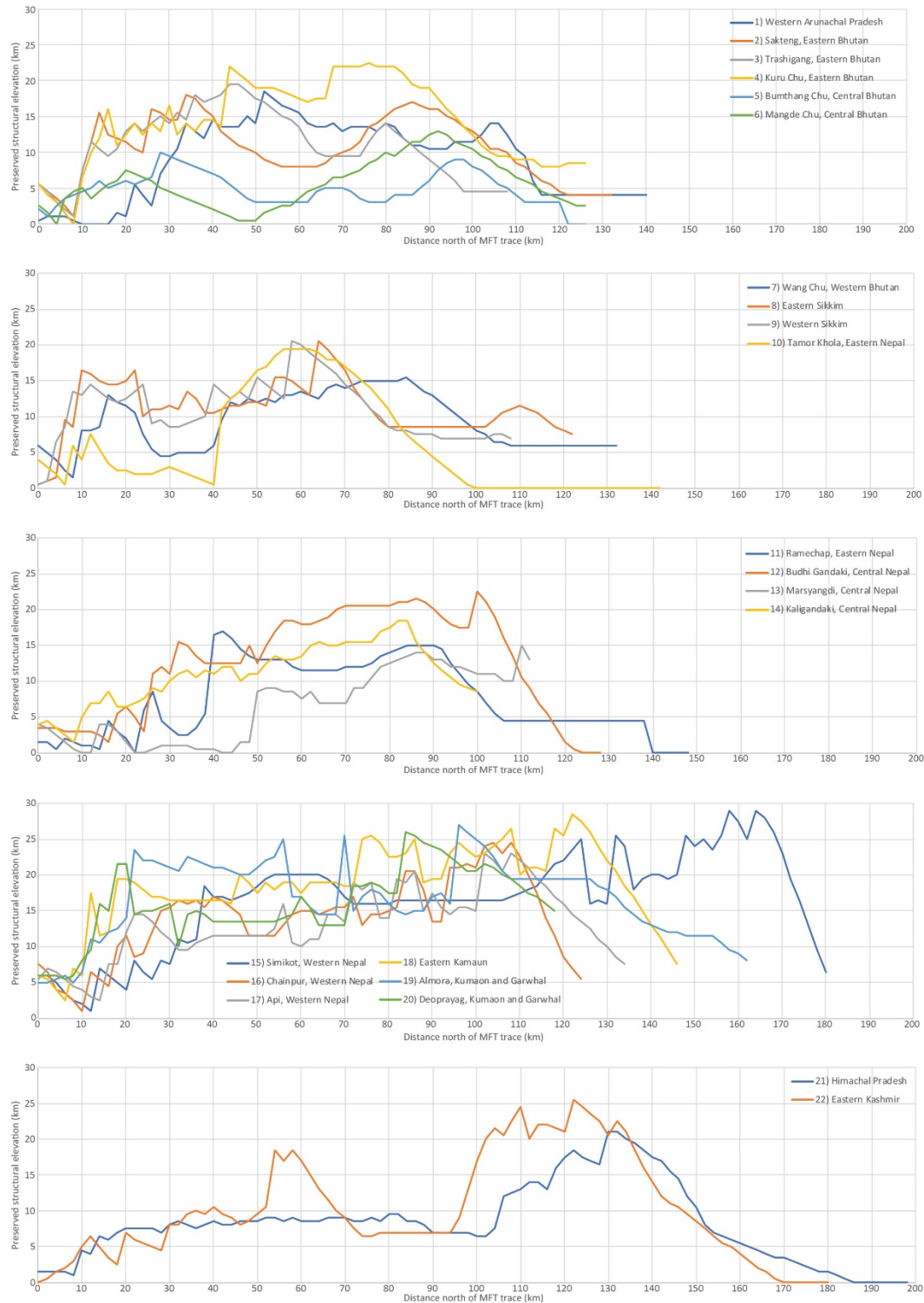


Figure DR5: Graphs of the preserved structural elevation (measured by comparing the elevation of the LH-SH stratigraphic level exposed at the modern surface to its elevation at or below the basal décollement) accomplished by the LH-SH thrust belt versus distance N of the MFT trace for each of the 22 cross sections. The data used to make these graphs are shown in Table DR4.



REFERENCES CITED

- Bhat, G.M., Ram, G., and Koul, S., 2009, Potential for oil and gas in the Proterozoic carbonates (Sirban Limestone) of Jammu, northern India: Geological Society of London Special Publication 326, p. 245-254, doi: 10.1144/SP326.14
- Bhattacharyya, K., Mitra, G., and Kwon, S., 2015, Geometry and kinematics of the Darjeeling–Sikkim Himalaya, India: Implications for the evolution of the Himalayan fold-thrust belt: *Journal of Asian Earth Sciences*, v. 113, p. 778–796, doi: 10.1016/j.jseaes.2015.09.008.
- DeCelles, P.G., Carrapa, B., Gehrels, G.E., Chakraborty, T., and Ghosh, P., 2016, Along-strike continuity of structure, stratigraphy, and kinematic history in the Himalayan thrust belt: The view from northeastern India: *Tectonics*, v. 35, p. 2995–3027, doi: 10.1002/2016TC004298.
- Gavillot, Y., Meigs, A.J., Sousa, F.J., Stockli, D., Yule, D., and Malik, M., 2018, Late Cenozoic foreland-to-hinterland low-temperature exhumation history of the Kashmir Himalaya: *Tectonics*, v. 37, p. 3041-3068, doi: 10.1029/2017TC004668.
- Khanal, S., 2014, Structural and kinematic evolution of the Himalayan thrust belt, central Nepal: [Ph.D. Dissertation], University of Alabama, Tuscaloosa, 185 p., 37 figures, 8 tables.
- Khanal, S., and Robinson, D.M., 2013, Upper crustal shortening and forward modeling of the Himalayan thrust belt along the Budhi-Gandaki River, central Nepal: *International Journal of Earth Sciences*, v. 102, p. 1871–1891, doi: 10.1007/s00531-013-0889-1.
- Long, S., McQuarrie, N., Tobgay, T., and Grujic, D., 2011a, Geometry and crustal shortening of the Himalayan fold-thrust belt, eastern and central Bhutan: *Geological Society of America Bulletin*, v. 123, p. 1427-1447, doi:10.1130/B30203.1.
- Long, S.P., McQuarrie, N., Tobgay, T., Grujic, D., and Hollister, L., 2011b, Geologic map of Bhutan: *The Journal of Maps*, v2011, p. 184-192, 1:500,000-scale, doi: 10.4113/jom.2011.1159.

Long, S.P., Gordon, S.M., and Soignard, E., 2017, Distributed north-vergent shear and flattening through Greater and Tethyan Himalayan rocks: insights from metamorphic and strain data from the Dang Chu region, central Bhutan: *Lithosphere*, v. 9, p. 774-795, doi: 10.1130/L655.1.

Mandal, S., Robinson, D.M., Kohn, M.J., Khanal, S., and Das, O., 2019, Examining the tectono-stratigraphic architecture, structural geometry, and kinematic evolution of the Himalayan fold-thrust belt, Kumaun, northwest India: *Lithosphere*, v. 11, p. 414-435, doi: 10.1130/L1050.1.

Martin, A. J., Burg, K.D., Kaufman, A.J., and Gehrels, G.E., 2011, Stratigraphic and tectonic implications of field and isotopic constraints on depositional ages of Proterozoic Lesser Himalayan rocks in central Nepal: *Precambrian Research*, v. 185, p. 1–17, doi: 10.1016/j.precamres.2010.11.003.

McQuarrie, N., Tobgay, T., Long, S.P., Reiners, P.W., and Cosca, M.A., 2014, Variable exhumation rates and variable displacement rates: Documenting recent slowing of Himalayan shortening in western Bhutan: *Earth and Planetary Science Letters*, v. 386, p. 161–174, doi: 10.1016/j.epsl.2013.10.045.

McQuarrie, N., Eizenhöfer, P.R., Long, S.P., Tobgay, T., Ehlers, T., Reiners, P.W., Blythe, A., Morgan, L., Gilmore, M., and Dering, G., 2019, The influence of foreland structures on hinterland cooling: evaluating the drivers of exhumation in the Eastern Bhutan Himalaya: *Tectonics*, v. 38, p. 3282-3310, doi: 10.1029/2018TC005340.

Parui, C., and Bhattacharyya, K., 2018, Duplex and along-strike structural variation: A case study from Sikkim Himalayan fold thrust belt: *Journal of Structural Geology*, v. 113, p. 62–75, Doi: 10.1016/j.jsg.2018.05.017.

Robinson, D.M., DeCelles, P.G., and Copeland, P., 2006, Tectonic evolution of the Himalayan thrust belt in western Nepal: implications for channel flow models: *Geological Society of America Bulletin*, v. 118, p. 865-885, doi: 10.1130/B25911.1.

Robinson, D.M., and Martin, A.J., 2014, Reconstructing the Greater Indian margin: A balanced cross section in central Nepal focusing on the Lesser Himalayan duplex: *Tectonics*, v. 33, p. 2143–2168, doi: 10.1002/2014TC003564.

Schelling, D., 1992, The tectonostratigraphy and structure of the eastern Nepal Himalaya: *Tectonics*, v. 11, no. 5, p. 925-943, doi: 10.1029/92TC00213.

Schelling, D., and Arita, K., 1991, Thrust tectonics, crustal shortening, and the structure of the far-eastern Nepal Himalaya: *Tectonics*, v. 10, no. 5, p. 851-862, doi: 10.1029/91TC01011.

Schneider, C.A., Rasband, W.S., and Eliceiri, K.W., 2012, NIH Image to ImageJ: 25 years of image analysis: *Nature Methods*, v. 9, p. 671-675.

Srivastava, P., and Mitra, G., 1994, Thrust geometries and deep structure of the outer and lesser Himalaya, Kumaon and Garwal (India): Implications for evolution of the Himalayan fold-and-thrust belt: *Tectonics*, v. 13, p. 89-109, doi: 10.1029/93TC01130.

Webb, A.A.G., 2013, Preliminary balanced palinspastic reconstruction of Cenozoic deformation across the Himachal Himalaya (northwestern India): *Geosphere*, v. 9, p. 572–587, doi: 10.1130/GES00787.1.